HEALTH AND MEDICINE

Copyright © 2020 The Authors, some rights reserved; exclusive licensee American Association for the Advancement of Science. No claim to original U.S. Government Works. Distributed under a Creative Commons Attribution NonCommercial License 4.0 (CC BY-NC).

Transient stealth coating of liver sinusoidal wall by anchoring two-armed PEG for retargeting nanomedicines

Anjaneyulu Dirisala[1]*, Satoshi Uchida[1,2*†], Kazuko Toh[1], Junjie Li[1], Shigehito Osawa[1,3], Theofilus A. Tockary[1], Xueying Liu[1], Saed Abbasi[1], Kotaro Hayashi[1], Yuki Mochida[1], Shigeto Fukushima[1], Hiroaki Kinoh[1], Kensuke Osada[4], Kazunori Kataoka[1,5†]

A major critical issue in systemically administered nanomedicines is nonspecific clearance by the liver sinusoidal endothelium, causing a substantial decrease in the delivery efficiency of nanomedicines into the target tissues. Here, we addressed this issue by in situ stealth coating of liver sinusoids using linear or two-armed poly(ethylene glycol) (PEG)–conjugated oligo(L-lysine) (OligoLys). PEG-OligoLys selectively attached to liver sinusoids for PEG coating, leaving the endothelium of other tissues uncoated and, thus, accessible to the nanomedicines. Furthermore, OligoLys having a two-armed PEG configuration was ultimately cleared from sinusoidal walls to the bile, while OligoLys with linear PEG persisted in the sinusoidal walls, possibly causing prolonged disturbance of liver physiological functions. Such transient and selective stealth coating of liver sinusoids by two-arm-PEG-OligoLys was effective in preventing the sinusoidal clearance of nonviral and viral gene vectors, representatives of synthetic and nature-derived nanomedicines, respectively, thereby boosting their gene transfection efficiency in the target tissues.

INTRODUCTION

Nanomedicines have been widely studied for the efficient delivery of therapeutic and diagnostic agents into target tissues (*1*–*6*). However, nanomedicines are exposed to several clearance mechanisms, such as reticuloendothelial system (RES) uptake, after their systemic administration (*7*–*9*). Among these mechanisms, liver sinusoidal endothelial cells (LSECs) express numerous types of scavenger receptors for capturing a variety of nanomedicines and have high endocytic activity to clear them actively from the blood circulation (*10*–*12*). The targets of LSEC-mediated clearance include both synthetic and nature-derived nanomedicines, such as viral gene vectors (*13*, *14*), limiting their delivery efficiency to the target tissues.

To address this issue of LSEC-mediated clearance, the stealth coating of nanomedicines, e.g., by poly(ethylene glycol) (PEG), which allows nanomedicines to persist in the blood circulation for hours to days, has been widely attempted (*15*–*18*). However, depending on the formulation of the nanomedicine and its drug contents, it is often difficult to obtain sufficient stealth coating to completely inhibit the clearance mechanisms without compromising nanomedicine functionality (*19*–*22*). Thus, a combination of other strategies is required. The modulation of host-tissue clearance mechanisms is a promising option. For this purpose, previous studies have attempted to saturate the availability of clearing sites, e.g., by preinjecting scavenger receptor ligands, such as fucoidan (*23*), polyinosinic acid (poly-I) (*24*), and dextran sulfate (DS) (*25*), or decoy nanoparticles, such as polymer-albumin nanoparticles (*26*) and cationic liposomes (*27*). However, this strategy has two major problems. First, agents used for receptor saturation inhibit only specific mechanisms of sinusoidal clearance, depending on the receptors or clearance sites that they target, despite the fact that the liver sinusoid has diverse clearance pathways. Even a single nanomedicine can be recognized by several receptors (*12*, *28*, *29*), such that the simultaneous inhibition of various clearance mechanisms is preferred. Second, the receptor saturation strategy often raises safety concerns, including inflammatory responses induced by fucoidan (*30*) or poly-I (*31*) and anticoagulation associated with the administration of DS (*32*).

To circumvent these issues, herein we propose transient and selective stealth coating of liver sinusoidal endothelium, using precisely designed PEGylated oligocation (Fig. 1). In contrast to the previous strategy of receptor saturation, PEG coating of liver sinusoidal endothelium would be effective for the simultaneous inhibition of various clearance mechanisms. The coating should be transient and selective to the liver sinusoid to avoid toxicity concerns. This was achieved by using oligo(L-lysine) (OligoLys) conjugated with two-armed PEG at its carboxyl end (two-arm-PEG-OligoLys) for anchoring PEG to liver sinusoidal walls. The PEGylation of OligoLys allowed us to avoid the nonspecific attachment of OligoLys to the extra-liver endothelium, presumably via the steric repulsion of PEG, with preserved binding capability to liver sinusoidal endothelium, which may have high binding affinity to oligocations because of the abundance of heparan sulfate proteoglycans and scavenger receptors (*11*, *33*, *34*). The clearance behavior of the PEGylated OligoLys was successfully controlled by optimizing the PEG configuration, with two-arm-PEG-OligoLys showing transient PEG coating to the liver sinusoidal endothelium, followed by gradual biliary clearance, while the OligoLys conjugated with one-armed (linear) PEG (one-arm-PEG-OligoLys) bound to the sinusoidal endothelium persistently. Subsequently, transient and selective stealth coating of liver sinusoids

[1]Innovation Center of NanoMedicine, Kawasaki Institute of Industrial Promotion, 3-25-14 Tonomachi, Kawasaki-ku, Kawasaki 210-0821, Japan. [2]Department of Bioengineering, Graduate School of Engineering, The University of Tokyo, 7-3-1 Hongo, Bunkyo-ku, Tokyo 113-8656, Japan. [3]Department of Applied Chemistry, Faculty of Science, Tokyo University of Science, 1-3 Kagurazaka, Shinjuku-ku, Tokyo 162-8601, Japan. [4]National Institutes for Quantum and Radiological Science and Technology, 4-9-1 Anagawa, Inage-ku, Chiba 263-8555, Japan. [5]Institute for Future Initiatives, The University of Tokyo, 7-3-1 Hongo, Bunkyo-ku, Tokyo 113-0033, Japan.
*These authors contributed equally to this work.
†Corresponding author. Email: suchida@bmw.t.u-tokyo.ac.jp (S.U.); kataoka@ifi.u-tokyo.ac.jp (K.K.)

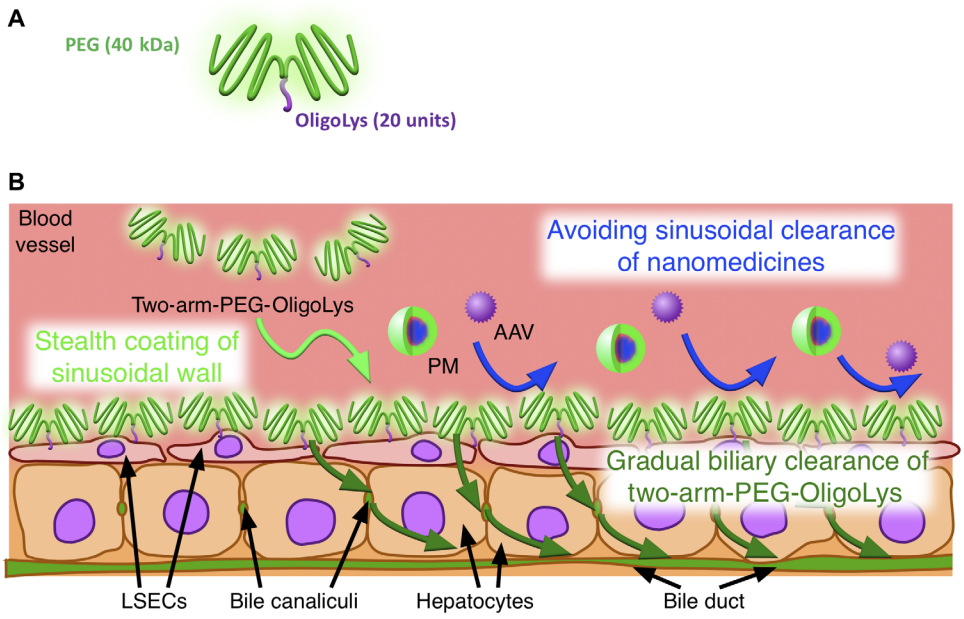

Fig. 1. In situ stealth coating of liver sinusoidal wall using PEG-OligoLys. (**A**) OligoLys with 20 Lys units conjugated with two linear chains of 40-kDa PEG at its carboxyl end (two-arm-PEG-OligoLys). (**B**) Schematic illustration of in situ stealth coating of liver sinusoidal wall. Two-arm-PEG-OligoLys selectively attaches to the sinusoidal wall to prevent the attachment of nanomedicines, such as polyplex micelle (PM) and adeno-associated virus (AAV), to the wall via stealth property of PEG. Two-arm-PEG-OligoLys is gradually cleared to the bile to avoid prolonged disturbance of liver sinusoid functions.

by two-arm-PEG-OligoLys was found to be effective in preventing the sinusoidal clearance of nonviral and viral gene vectors, providing an increased gene transfection efficiency in their target tissues via their relocation from the liver sinusoid to the tissues.

RESULTS

Selective coating of liver sinusoidal wall using PEGylated OligoLys

Short OligoLys with approximately 20 Lys units was used, as the shortening of the oligo-polycation is an effective strategy to circumvent toxicity concerns (*35*, *36*). OligoLys was PEGylated in two different methods, using either one- or two-armed PEG. A single linear chain of 80-kDa PEG or double linear chains of 40-kDa PEG were conjugated to OligoLys at the proximal ω-NH_2 terminus of PEG by forming a stable covalent amide bond to the distal carboxyl end of OligoLys (Fig. 2A). We selected the PEGylated OligoLys samples to have the same total M_w (weight-average molecular weight) of PEG in each molecule, i.e., 80 kDa. Total PEG M_w was set to 80 kDa for avoiding renal clearance of PEGylated OligoLys (*37*), which may influence its sinusoidal coating behavior. Note that each molecule of two-arm-PEG-OligoLys has two 40-kDa PEG strands, meaning that total M_w of PEG per OligoLys strand in the molecule is set at 80 kDa, and this is the same PEG M_w ratio to OligoLys as that in each of the one-arm-PEG-OligoLys molecule with a single strand of 80-kDa PEG. In this way, we can faithfully evaluate the effect of PEG configuration (linear versus two-arm branched) without an influence of total M_w of PEG fraction in each PEGylated OligoLys molecule. These PEGylated OligoLys formulations were labeled with a single molecule of Alexa Fluor 594 at the OligoLys main chain ω-NH_2 group for the real-time fluorescence observation of their pharmacokinetic behaviors in living mice using intravital confocal laser scanning microscopy (IVCLSM).

When observing the earlobe dermis, a representative connective tissue, after intravenous injection of one- and two-arm-PEG-OligoLys, the fluorescence intensity of the blood vessel walls was comparable with that of the lumen (Fig. 2, B and C), indicating no PEGylated OligoLys attachment to the vessel walls of the earlobe. On the contrary, non-PEGylated OligoLys with approximately 28 Lys units was aligned to the vessel walls of the earlobe as early as 5 min after injection (Fig. 2D). Thus, the attachment of OligoLys to the vessel walls of a connective tissue was successfully avoided by PEGylation of OligoLys, presumably due to stealth properties of PEG.

In sharp contrast, both one- and two-arm-PEG-OligoLys were attached to the vessel walls of the liver sinusoid within 5 min after injection (Fig. 3, A and B). Quantitative analysis revealed a much higher fluorescence intensity of the sinusoidal wall compared with the lumen (Fig. 3, C and D). This observation indicates the successful PEG coating of the liver sinusoidal wall after the injection of one- and two-arm-PEG-OligoLys. These PEGylated OligoLys formulations attached more efficiently to the blood vessel walls of the liver compared with those of the connective tissue (Fig. 2, B and C). Such selective binding of one- and two-arm-PEG-OligoLys to the liver sinusoidal wall may be attributed to the abundancy of anionic proteoglycans, such as heparan sulfate proteoglycans, present on the sinusoidal extracellular matrix, which can capture oligocations (*33*, *34*), as well as to the high expression levels of scavenger receptors, which recognize cationic macromolecules, on sinusoidal cells (*11*).

Biliary clearance of PEGylated OligoLys

The two-arm-PEG-OligoLys fluorescence signal at the sinusoidal wall gradually decreased and became almost undetectable at 6 hours or later after injection (Fig. 3, B and D), whereas one-arm-PEG-OligoLys remained localized to the sinusoidal wall even at 9 hours after injection, with a minimal decrease in the fluorescence intensity of the sinusoidal wall during the observation period (Fig. 3, A and C). Closer

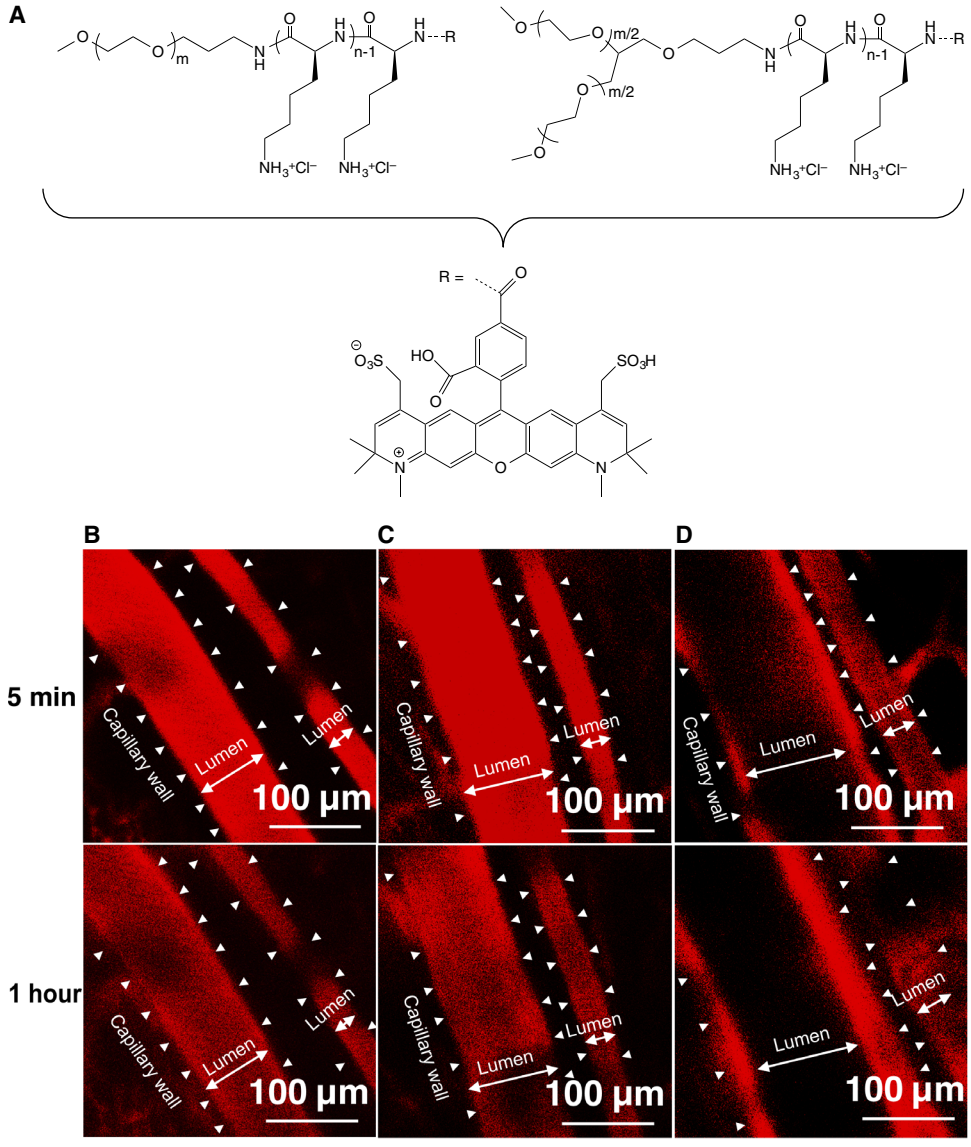

Fig. 2. OligoLys distribution in connective tissue. (**A**) Chemical structures of one-arm-PEG-OligoLys (top, left), two-arm-PEG-OligoLys (top, right) with or without Alexa594 labeling (bottom). (**B** to **D**) Alexa594-labeled OligoLys with or without PEGylation was intravenously injected. Five minutes or 1 hour after the injection, earlobe dermis was observed using IVCLSM. (B) One-arm-PEG-OligoLys. (C) Two-arm-PEG-OligoLys. (D) Non-PEGylated OligoLys. Arrowheads, capillary walls. Two-way arrows, capillary lumen.

observation revealed that two-arm-PEG-OligoLys was progressively accumulated to the space between the hepatocytes (encircled with dotted lines in Fig. 3B) at 3 hours or later after injection, whereas one-arm-PEG-OligoLys exhibited an almost undetectable accumulation to that space even at 9 hours after injection. On the basis of its anatomical position, the space may correspond to the bile canaliculi, which collect the bile from hepatocytes for clearance through the bile ducts. To clarify this point, a fluorescent bile tracer, 5-carboxyfluorescein (CF), was injected 5 min before two-arm-PEG-OligoLys injection. The position of two-arm-PEG-OligoLys accumulation at 7 hours after injection was colocalized with that of CF, as observed in the white or cyan pixels in Fig. 3E, which resulted from the merging of green (CF) and magenta pixels (two-arm-PEG-OligoLys). These observations indicate the gradual biliary clearance of two-arm-PEG-OligoLys.

The clearance profile of one- and two-arm-PEG-OligoLys was additionally evaluated by observing their persistence in the blood circulation. While these two groups showed comparable blood circulation profile within 1 hour after injection, obvious differences were observed at 1 hour or later after injection (Fig. 3F); the blood concentration of two-arm-PEG-OligoLys gradually decreased, while that of one-arm-PEG-OligoLys remained almost constant. The blood concentrations of one- and two-arm-PEG-OligoLys fit the two-compartment model with high R^2 values, in which the polymers were administered into the central compartment and subsequently distributed into a tissue compartment (fig. S1 and table S1). These two formulations showed a comparable distribution phase half-life of around 15 min, with a comparable distribution rate constant (k_{12}). This is consistent with the observation that both formulations similarly showed rapid binding to hepatic sinusoids. On the

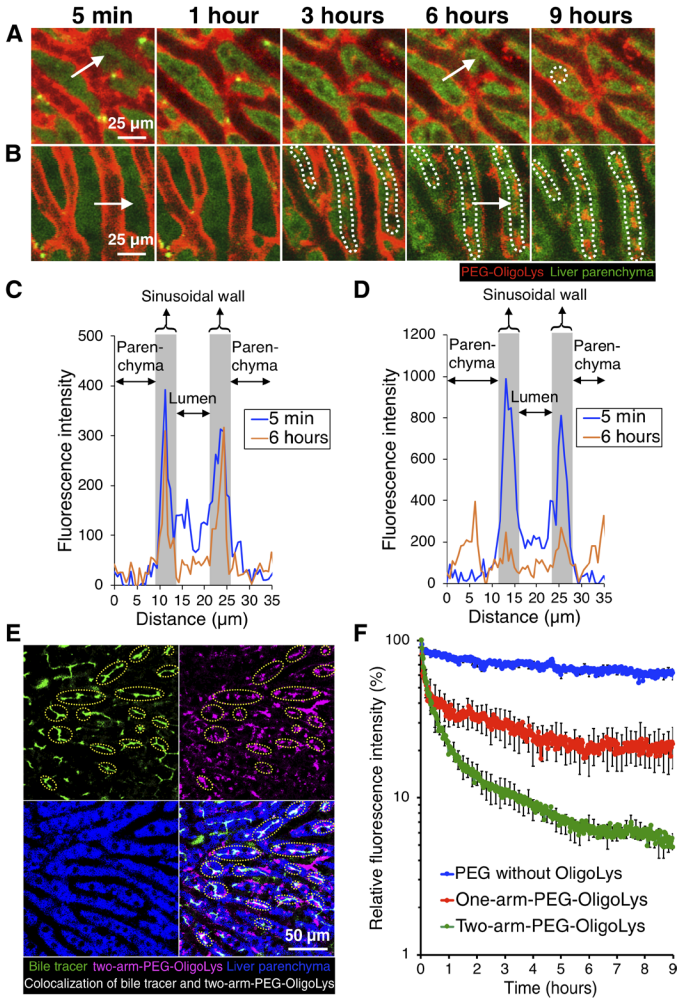

Fig. 3. Attachment of PEG-OligoLys to liver sinusoidal wall and its clearance. (**A** to **D**) IVCLSM images after injection of Alexa594-labeled one-arm-PEG-OligoLys (A) and two-arm-PEG-OligoLys (B). Green, autofluorescence of liver parenchyma. Red, one- and two-arm-PEG-OligoLys. Presumable regions of bile canaliculi are encircled with white dotted lines. Intensity profiles of Alexa594 in the white arrows in (A) and (B) are shown in (C) and (D), respectively. (C) One-arm-PEG-OligoLys. (D) Two-arm-PEG-OligoLys. (**E**) Bile ducts were visualized using 5-carboxyfluorescein (CF, green). Then, Alexa594-labeled two-arm-PEG-OligoLys (magenta) was injected for observation 7 hours later. Colocalization of these two colors is observed as white or cyan (encircled by yellow dotted lines). (**F**) Blood circulation profiles of PEG without OligoLys, and one- and two-arm-PEG-OligoLys. $n = 4$. Data are shown as means ± SEM.

other hand, the elimination phase half-life of one-arm-PEG-OligoLys (13.3 hours) was much longer than that of two-arm-PEG-OligoLys (5.7 hours), which may reflect the different clearance behaviors of these two groups. The blood circulation profile of PEG without OligoLys conjugation fits the one-compartment model with high R^2 values and presented a long half-life (19.8 hours). Without binding to vessel walls, this formulation may lack a distribution phase.

To obtain further mechanistic insights into the different behaviors between one- and two-arm-PEG-OligoLys, these two formulations were coinjected into mice for IVCLSM observation of their distribution in the hepatic sinusoids after labeling one-arm-PEG-OligoLys with Alexa647 (fig. S2, red) and two-arm-PEG-OligoLys with Alexa594 (green). Both formulations showed comparable levels of liver sinusoidal accumulation at 5 min to 1 hour after injection (Fig. 4 and movie S1). This observation suggests that the binding affinity of these formulations to the sinusoids is comparable. In sharp contrast, fluorescence from two-arm-PEG-OligoLys in the sinusoidal wall became weak, especially 6 hours or later after injection, presumably through biliary clearance, while a strong fluorescence signal from one-arm-PEG-OligoLys was consistently observed in the wall. Eventually, the sinusoidal walls in the images gradually became red (one-arm-PEG-OligoLys), with green (two-arm-PEG-OligoLys) appearing in the presumable location of the bile canaliculi 6 hours or later after injection. This observation is consistent with that after the single injection of each formulation, with two-arm-PEG-OligoLys still gradually cleared in the presence of one-arm-PEG-OligoLys. Thus, one-arm-PEG-OligoLys may preserve the liver functionality of biliary clearance but failed to be cleared under these conditions.

Toward safe usage of two-arm-PEG-OligoLys, it is important to estimate its clearance rate. For this purpose, blood clearance profile of two-arm-PEG-OligoLys was observed under its continuous intravenous infusion. In this experiment, bolus intravenous injection of two-arm-PEG-OligoLys was performed at a dose of 1250 μg per mouse, which is the same as that used throughout this study. Subsequently, two-arm-PEG-OligoLys was infused at the rate reduced in a stepwise manner, to find the rate that allows the blood level of two-arm-PEG-OligoLys to be constant. Under such condition, the infusion rate of two-arm-PEG-OligoLys would be balanced with its clearance rate. The blood level of two-arm-PEG-OligoLys was constant under the infusion rate of 1200 μg/hour per mouse and gradually decreased under the rate of 630 μg/hour per mouse (fig. S3). This result suggests that the clearance rate of two-arm-PEG-OligoLys was approximately 1200 μg/hour per mouse. This clearance may occur mainly through the biliary pathway, as two-arm-PEG-OligoLys with molecular weight over 80 kDa is unlikely to be cleared through the renal pathway. Two-arm-PEG-OligoLys accumulation to the bile canaliculi was observed in intravital observation of the liver 3 hours or later after the injection (Fig. 3B). It is also worthy to note that the biliary clearance rate of two-arm-PEG-OligoLys (1200 μg/hour per mouse = 240 pmol/min per mouse) is comparable with that of cationic drugs (100 to 1000 pmol/min per mouse), as reported previously (*38*).

We then checked hemolysis and change in major biomarkers related to liver and kidney functions to estimate potential acute toxicity of injected polymers. Two-arm-PEG-OligoLys, as well as one-arm-PEG-OligoLys, showed no ex vivo hemolytic activity (fig. S4) and no detectable changes in plasma levels of a general tissue damage marker [lactate dehydrogenase (LDH)], liver damage markers [aspartate aminotransaminase (AST) and alanine aminotransferase (ALT)], and kidney function markers [blood urea nitrogen (BUN) and creatinine (Cre)] after in vivo administration (table S2). On the other hand, non-PEGylated OligoLys induced a substantial level of hemolysis activity ex vivo and LDH release in vivo.

Together, the above results demonstrate that the clearance behavior of the PEGylated OligoLys was successfully controlled by fine-tuning of PEG configuration. PEGylated OligoLys formulations used for the transient stealth coating of liver sinusoidal wall should simultaneously meet the following two requisites: (i) sufficient and selective stealth coating of the liver sinusoidal wall for retargeting nanomedicines and (ii) ensured clearance from the sinusoidal wall for avoiding chronic disturbance of physiological functions due to accumulation

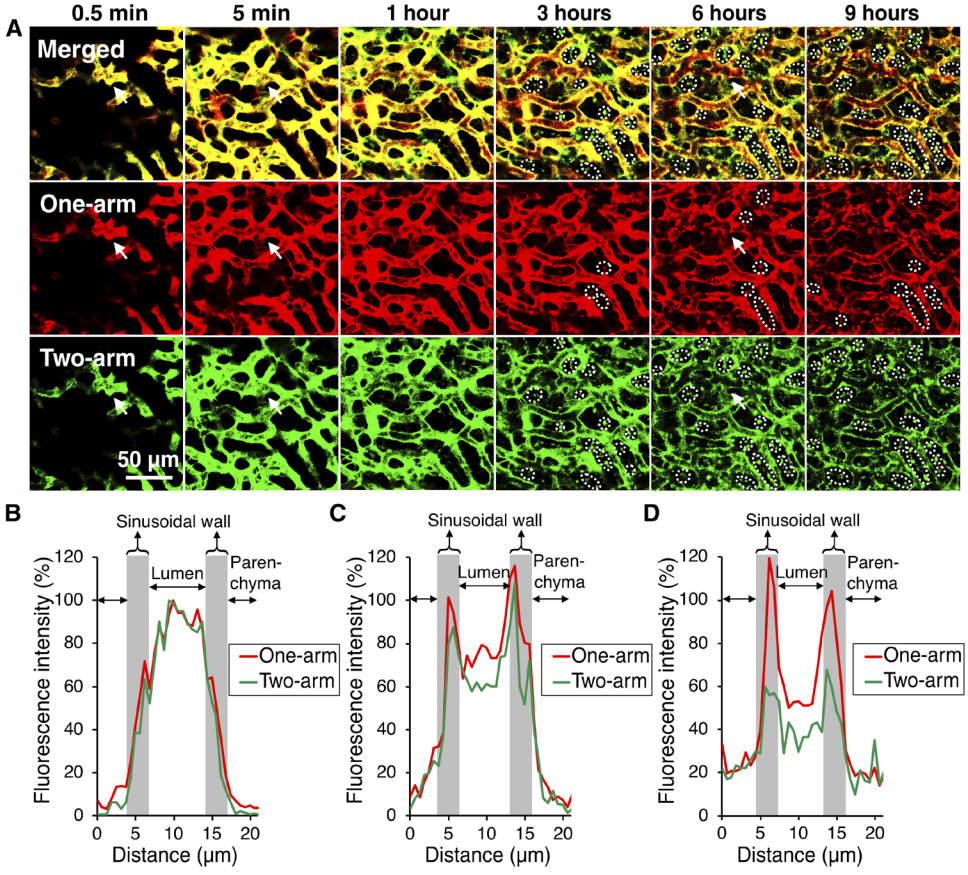

Fig. 4. Coinjection of one- and two-arm-PEG-OligoLys. Alexa647-labeled one-arm-PEG-OligoLys (red) and Alexa594-labeled two-arm-PEG-OligoLys (green) were co-injected from the tail vein. (**A**) IVCLSM imaging of the liver. Presumable regions of bile canaliculi are encircled with white dotted lines. (**B** to **D**) Intensity profiles of Alexa594 and Alexa647 in the white arrows shown in (A). (B) 0.5 min, (C) 5 min, and (D) 6 hours after injection.

of PEG-OligoLys in the body. As shown in Figs. 2 and 3, both one- and two-arm-PEG-OligoLys attached to the sinusoidal walls selectively, meeting requisite (i). Worth noting is that two-arm-PEG-OligoLys was able to be cleared from the sinusoidal wall to the bile in several hours, while one-arm-PEG-OligoLys persisted on the wall even after 9 hours of the observation period. This result indicates that one-arm-PEG-OligoLys does not satisfy requisite (ii), which may induce safety concerns of chronic accumulation toxicity. Thus, we selected only two-arm-PEG-OligoLys for further examination devoted to evaluate redirecting efficacy of nanomedicines, demonstrating the enhanced gene expression of polyplex micelle (PM) and adeno-associated virus (AAV) in target tissues as described in the following sections.

Retargeting of pDNA nanoparticles from the liver sinusoid to the tumor

To evaluate the feasibility of the sinusoidal PEG coating strategy, we first selected PM loading plasmid DNA (pDNA) as a model nanomedicine (*39*, *40*). PM was prepared by mixing pDNA with one-arm-PEG-poly(L-lysine) (PLys) block copolymers with a PEG M_w of 12 kDa and a PLys polymerization degree of 44, installed with thiol moieties in 50% of the lysine residues for environment-responsive cross-linking between the cationic segments of the block copolymers. The PM was composed of a PEG shell and a core containing condensed pDNA. Disulfide cross-linking in the core stabilizes PM in extracellular environments and is selectively cleaved in intracellular reductive environments for pDNA release. According to our previous report, despite the stealth and stabilized PM formulation, a large fraction of the PM was cleared from the blood circulation within 1 hour after systemic injection, with only 23% of the dose remaining in the blood at 1 hour after injection (*40*). Such a moderate level of stealthiness provides us with a good platform for the application of the sinusoidal PEG coating strategy to prolong the persistence of PM in the blood circulation.

PM showed a cumulant diameter of 112 nm with a polydispersity index (PDI) of 0.15 and an almost neutral ζ-potential of −1.5 mV, suggesting the successful formation of the core-shell structure, composed of a PEG shell and a core containing condensed pDNA. First, PM loading Cy5-labeled pDNA was intravenously injected into the mice without two-arm-PEG-OligoLys injection for IVCLSM observation of PM behavior in the liver. PM showed sinusoidal entrapment as early as 5 min after injection, despite the fact that PM was PEGylated (Fig. 5, A and C). When two-arm-PEG-OligoLys was preinjected into the mice 5 min before the PM injection, the sinusoidal entrapment of the PM was effectively prevented even at 1 hour after injection (Fig. 5, B and D). This process was more obviously visualized by labeling both of two-arm-PEG-OligoLys and PM, using Alexa594 for two-arm-PEG-OligoLys and Cy5-labeled pDNA for PM (fig. S5 and movie S2). Meanwhile, under continuous observation,

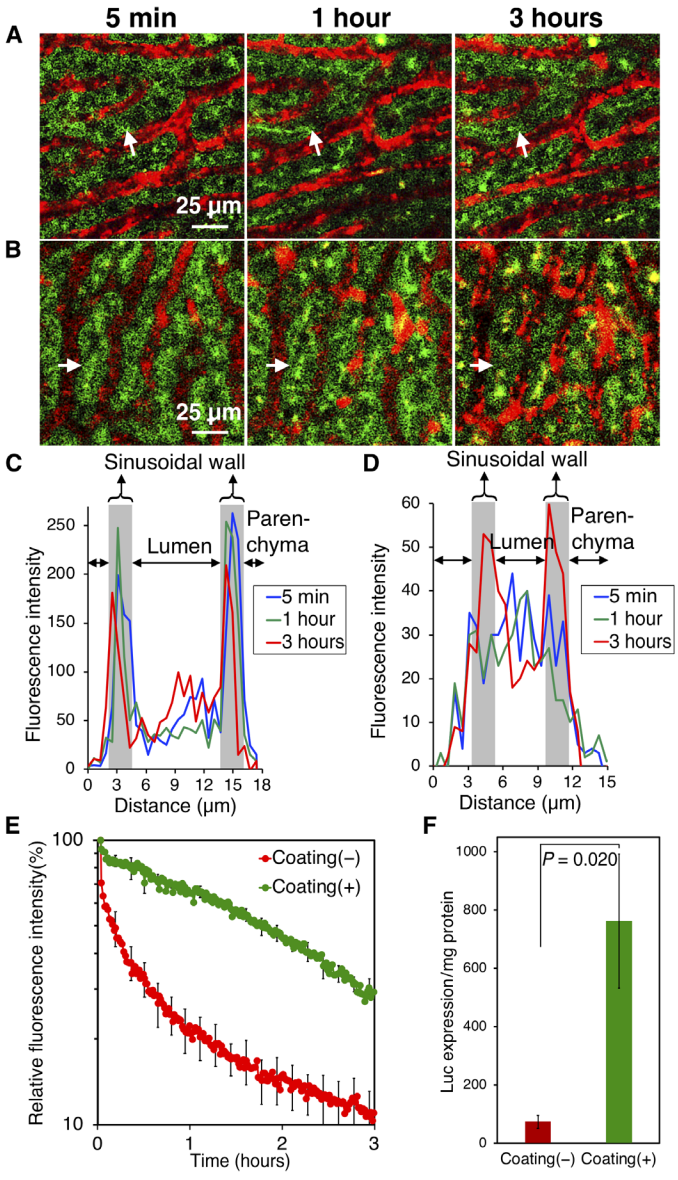

Fig. 5. Delivery of pDNA PM after preinjection of two-arm-PEG-OligoLys. Two-arm-PEG-OligoLys was intravenously injected to coat liver sinusoidal wall with PEG, followed by the intravenous injection of PM loading pDNA 5 min later. (**A** and **B**) IVCLSM imaging of PM loading Cy5-labeled pDNA (red) in the liver without PEG coating of sinusoid (A) or with the coating (B). Intensity profiles of Cy5 in the white arrows in (A) and (B) are shown in (**C**) and (**D**), respectively [(C) without coating and (D) with coating]. (**E**) Blood circulation profiles of PM with or without PEG coating of sinusoidal wall. $n = 4$. (**F**) PM loading Luc-expressing pDNA was injected to tumor-bearing mice with or without preinjection of two-arm-PEG-OligoLys. Luc expression in the tumor was measured 2 days after injection. $n = 4$. Data are shown as means ± SEM. Statistical analysis was performed using unpaired two-tailed Student's *t* test.

PM preinjected with two-arm-PEG-OligoLys exhibited sinusoidal attachment to some extent at 3 hours after injection. This result is consistent with the gradual clearance of two-arm-PEG-OligoLys from the sinusoidal wall 3 hours after injection (Fig. 3, B and D).

The effect of two-arm-PEG-OligoLys preinjection on PM clearance was further evaluated by observing the blood circulation profile of PM. Without two-arm-PEG-OligoLys preinjection, PM showed two phases of decrease in its blood concentration, with a rapid drop within 1 hour after injection, followed by a gradual decrease (Fig. 5E). The marked decrease in the PM blood concentration could be attributed to its tissue distribution, including the sinusoidal entrapment, as shown in Fig. 5, A and C. Such rapid PM clearance from the blood was effectively prevented by two-arm-PEG-OligoLys preinjection, presumably via the prevention of sinusoidal PM clearance, as shown in Fig. 5, B and D.

These promising results motivated us to use our strategy for gene transfection at the tumor site, as the PM formulation used in this study provided successful outcomes in the antiangiogenic treatment of cancer in our previous reports (*41*, *42*). PM loading *luciferase* (*Luc*) pDNA was intravenously injected into the mice bearing C26 murine colon carcinoma, 5 min after preinjection of two-arm-PEG-OligoLys. Two-arm-PEG-OligoLys preinjection resulted in a more than 10-fold increase in Luc expression efficiency in the tumor compared with the PM injection without two-arm-PEG-OligoLys preinjection (Fig. 5F). The enhanced transfection expression efficiency of PM in the tumor after two-arm-PEG-OligoLys preinjection could be attributed to the avoidance of PM sinusoidal entrapment, which may result in enhanced tumor accumulation of PM.

Relocation of viral gene vectors from the liver sinusoid to their target organs

Last, we applied the two-arm-PEG-OligoLys preinjection approach to the administration of viral gene vectors, in which this technology is highly demanded. In particular, when organs other than the liver are targeted, sinusoidal entrapment of the vectors seriously hinders the ability of viruses to reach their target organs (*14*, *24*), resulting in an increase in the viral dose, which then poses a safety problem. Although AAV is widely believed to be safe, high levels of toxicity have been observed in large animals after AAV administration at the dose that is required to obtain therapeutic levels of protein expression in the spine (*43*). Here, two-arm-PEG-OligoLys preinjection was performed 5 min before injection with AAV8 to prevent the sinusoidal clearance of AAV8 and to relocate it to the heart and skeletal muscles, which are promising target organs for the therapeutic application of AAV8 (*44*). Three weeks after the delivery of AAV8 expressing Luc, two-arm-PEG-OligoLys preinjection resulted in a decrease in the expression efficiency of Luc in the liver to 42% of the level observed without two-arm-PEG-OligoLys preinjection (Fig. 6A). This result suggests the successful prevention of AAV8 entrapment in the liver by the PEG coating of the sinusoidal wall using two-arm-PEG-OligoLys. Two-arm-PEG-OligoLys preinjection resulted in a significant increase in Luc expression in AAV8 target organs, a 4.3-fold increase in the heart (Fig. 6B), and a 2.3-fold increase in the skeletal muscles (Fig. 6C), respectively, presumably via the relocation of AAV8 from the liver sinusoids to these organs after sinusoidal PEG coating. This result demonstrates the effectiveness of our strategy in increasing the gene expression of viral vectors in their target organs, which will allow for a reduction in the dose of the vectors needed for gene therapy, thereby minimizing the safety concerns.

DISCUSSION

An important feature of two-arm-PEG-OligoLys for future clinical applications is its transient binding profile to the liver sinusoidal walls with a gradual clearance to the bile, providing an advantage in

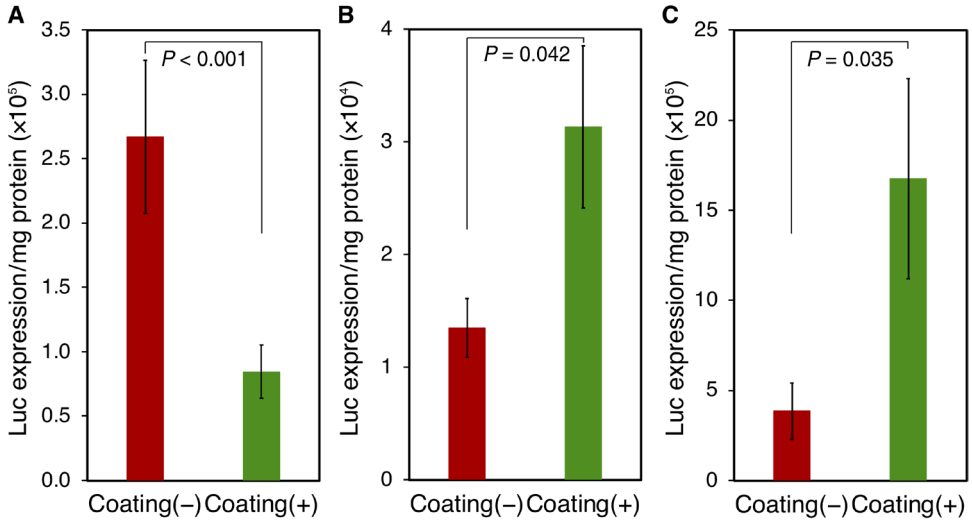

Fig. 6. AAV transfection after preinjection of two-arm-PEG-OligoLys. Five minutes after intravenous injection of two-arm-PEG-OligoLys for PEG coating of liver sinusoidal wall, AAV8 expressing Luc was intravenously injected. Three weeks later, Luc expression in the liver (**A**), heart (**B**), and skeletal muscle (**C**) was measured. $n = 6$. Data are shown as means ± SEM. Statistical analysis was performed using unpaired two-tailed Student's *t* test.

terms of safety over one-arm-PEG-OligoLys, which persisted in the sinusoidal wall. To obtain mechanistic insight into the differences between one- and two-arm-PEG-OligoLys, first, the intrinsic biliary excretion profile of OligoLys without PEGylation was observed in the liver using IVCLSM. Non-PEGylated OligoLys exhibited a high accumulation to the presumable location of bile canaliculi, especially 3 hours or more after injection (fig. S6). This result indicates that OligoLys is intrinsically cleared to the bile, while this process is inhibited by single 80-kDa PEG chain conjugation to OligoLys but not by double 40-kDa PEG chain conjugation. Meanwhile, both one- and two-arm-PEG-OligoLys exhibited similar behavior in terms of their binding to the sinusoidal wall after coinjection (Fig. 4). Thus, binding affinity to the sinusoidal wall may not be a major factor for the differences between one- and two-arm-PEG-OligoLys. Two-arm-PEG-OligoLys was cleared to the bile even after coinjection with one-arm-PEG-OligoLys, indicating that one-arm-PEG-OligoLys preserves the liver functionality of biliary clearance. Even under such conditions, one-arm-PEG-OligoLys still failed to be cleared.

Although detailed molecular analyses should be performed in the future to fully explain such clearance behavior of one- and two-arm-PEG-OligoLys, it is worth proposing a possible mechanism, based on the following two hypotheses. (i) Sinusoidal walls are densely coated with PEG. (ii) Biliary clearance of PEGylated OligoLys occurs via the endocytotic pathway, especially clathrin-mediated endocytosis, which is dominant in LSECs (*11*). On the basis of the radius of gyration, the diameter of 40-kDa and 80-kDa PEG is around 20 and 30 nm, respectively, which is close to the typical size of clathrin-coated vesicle (50 to 200 nm) (*45*, *46*). When cell membrane is densely coated with PEG, such large PEG chains would overlap with each other after curving of cell membrane in endocytosis, and such overlapping between PEG exclusion volume is entropically unfavorable based on a scaling theory (*47*, *48*). Here, we estimated the effect of PEG configuration on the overlapping volume using mathematical modeling, by assuming one-arm-PEG-OligoLys as one sphere of 80-kDa PEG and two-arm-PEG-OligoLys as two spheres of 40-kDa PEG, which densely coat the plasma membrane with a hexagonal lattice structure, without overlapping. In this model, curving of cell membrane in 50- to 200 nm-sized vesicles induces overlapping of PEG chains, with 80-kDa PEG providing more than threefold larger volume of the overlap compared with 40-kDa PEG (note S1). This calculation suggests that long single PEG chain (80 kDa) may not represent a suitable cargo of endocytotic vesicles to facilitate biliary excretion, while separation of PEG chains into two segments is effective in avoiding this issue.

Such transient coating of liver sinusoidal walls with two-arm-PEG-OligoLys allowed us to relocate nonviral and viral gene vectors from the sinusoidal wall to their target tissues, thereby improving the gene transfection efficiency in the tissues. With the ability to improve nanomedicine pharmacokinetics, this approach can be used not only to enhance the effect of nanomedicines but also to reduce the dose required to obtain these effects, which is particularly important for reducing the toxicity of viral gene therapy. While clearance behavior of two-arm-PEG-OligoLys was evaluated in detail after its single bolus administration as well as under the continuous infusion for several hours (fig. S3), detailed examination of possible chronic toxicity due to polymer overloading upon multiple injections may be required in the future to translate this procedure of transient surface covering of sinusoids in clinics, because nanomedicines are administered repeatedly in many cases. Here, we faithfully focus on the configuration of PEG (linear versus two-arm branched) having the same total M_w of 80 kDa, yet optimization of total PEG M_w should also be addressed in the future for further optimal tuning of the liver sinusoidal coating to maximize the efficacy of nanomedicine therapy, with minimal influence on liver physiological functions. Our approach is versatile for combinational use with various nanomedicines, including synthetic and nature-derived nanomedicines, opening avenues for future nanotherapy and nanodiagnosis.

MATERIALS AND METHODS

Synthesis and fluorescence labeling of OligoLys with or without PEGylation

OligoLys with or without PEGylation was synthesized via the ring-opening polymerization (ROP) of N^{ε}-trifluoroacetyl-L-lysine

N-carboxyanhydride [L-Lys(TFA)-NCA, Chuo Kaseihin Co. Inc., Tokyo, Japan], as previously described for two-arm-PEG-OligoLys (*49*), one-arm-PEG-OligoLys (*50*), and non-PEGylated OligoLys (*51*). Briefly, for two-arm-PEG-OligoLys synthesis, two-arm-α-methoxy-ω-amino-PEG [two-arm-PEG-NH_2, M_n (number-average molecular weight) = 2 × 40 kDa, NOF Corporation, Tokyo, Japan] was used as a macroinitiator for the ROP of L-Lys(TFA)-NCA to obtain two-arm-PEG-OligoLys(TFA). The molecular weight distribution (M_w/M_n) of two-arm-PEG-OligoLys(TFA) was 1.04, according to size exclusion chromatography (SEC) (TOSOH HLC-8220; Tosoh Corp., Tokyo, Japan). The TFA groups were deprotected to obtain two-arm-PEG-OligoLys. The degree of polymerization (DP) of OligoLys in two-arm-PEG-OligoLys was 19, according to ^{1}H nuclear magnetic resonance (NMR) spectrum (JEOL ECS 400; JEOL, Tokyo, Japan). For one-arm-PEG-OligoLys synthesis, one-arm-PEG-OligoLys(TFA) was synthesized using one-arm-α-methoxy-ω-amino-PEG (one-arm-PEG-NH_2, M_n = 83 kDa) as a macroinitiator of ROP of L-Lys(TFA)-NCA and exhibited M_w/M_n of 1.06 in SEC analysis. One-arm-PEG-OligoLys, obtained after the deprotection of TFA groups, showed an OligoLys DP of 21 in ^{1}H NMR. For non-PEGylated OligoLys synthesis, OligoLys(TFA) was synthesized by ROP of L-Lys(TFA)-NCA using *n*-butylamine (TCI Chemicals Co. Ltd., Tokyo, Japan) as an initiator, followed by the deprotection of TFA groups to obtain OligoLys. The DP of OligoLys was 28, according to the ^{1}H NMR spectrum. The fluorescence labeling of OligoLys with or without PEGylation was performed as previously described (*49*). Briefly, one- and two-arm-PEG-OligoLys and non-PEGylated OligoLys were labeled with a single molecule of Alexa dye at OligoLys at the main chain end the ω-NH_2 group before deprotecting the TFA groups using the *N*-hydroxysuccinimide (NHS) ester of Alexa Fluor 594 or 647 (Thermo Fischer Scientific, Waltham, MA, USA), according to the manufacturer's instructions. For injection, OligoLys with or without PEGylation, with or without fluorescence labeling, was dissolved in 10 mM Hepes buffer containing 150 mM NaCl (pH 7.3).

Ethical compliance for animal experiments

All animal experimental procedures were approved and conducted in compliance with the Institutional Guidelines for the Care and Use of Laboratory Animals as stated by the Animal Committee of the Innovation Center of NanoMedicine (iCONM).

Intravital observation of earlobe and liver

All of the intravital observations in this study were performed using IVCLSM, an A1R confocal laser scanning microscope (Nikon Corp., Tokyo, Japan), connected to an upright ECLIPSE FN1 (Nikon Corp.), using the following settings. The pinhole diameter was set to obtain a 10-μm optical slice. BALB/c mice (6 weeks old, female, 18 to 20 g, Charles River Laboratories Inc., Yokohama, Japan) were anesthetized with 2.5% isoflurane (Abbott Japan Co. Ltd., Tokyo, Japan) using a NARCOBIT-E Univenter 400 Anaesthesia Unit (Natsume Seisakucho Co. Ltd., Tokyo, Japan). The anesthetized mice were placed onto a temperature-controlled plate (Thermoplate; Tokai Hit Co. Ltd., Shizuoka, Japan) with the temperature set to 37°C.

For the observation of blood vessels in the earlobe dermis, the earlobe was fixed using a drop of immersion oil beneath the coverslip. For the observation of the liver, the liver was surgically exposed and glued directly to the cover glass using a drop of oil. Fluorescence-labeled OligoLys with or without PEGylation was intravenously injected through a catheter inserted into the lateral tail vein slowly in approximately 30 s at the dose of 15 nmol per mouse (1.25 mg per mouse for one- and two-arm-PEG-OligoLys and 0.05 mg per mouse for non-PEGylated OligoLys). Throughout the study, the autofluorescence signal of liver parenchyma was excited using a 405-nm laser and detected using a 450/50-nm bandpass emission filter. Alexa594 was excited using a 561-nm laser and detected using a 595/50 bandpass emission filter. Alexa647 was excited using a 640-nm laser and detected using a 700/50-nm bandpass emission filter. A 40× objective lens was used for liver imaging, while a 20× objective lens was used for earlobe imaging. Images were processed using NIS-Elements software (Nikon Corp.) for the quantification of fluorescence intensity. The fluorescence intensity of each pixel in the line charts was calculated after subtracting the background fluorescence intensity, which was measured using the images obtained 10 s before sample injection.

Bile duct imaging

CF diacetate (CFDA, TCI Chemicals Co. Ltd.) was intravenously injected at a dose of 0.2 mg/kg. Five minutes later, a liver image was obtained using IVCLSM, by exciting CFDA using a 488-nm laser and detecting the fluorescence using a 520/50-nm bandpass emission filter. Immediately after the CFDA imaging, two-arm-PEG-OligoLys was intravenously injected for liver imaging 7 hours later, as described in the previous section.

Evaluation of blood circulation profile

The blood circulation profile of fluorescence-labeled OligoLys with or without PEGylation was quantified by measuring the fluorescence intensity of the blood vessel lumen in the earlobe after injection of the samples, as described in our previous report (*49*). Briefly, the fluorescence intensity in the region of interest (ROI) in the vein was measured at each time point, followed by the subtraction of the background fluorescence intensity obtained 10 s before the injection. The value obtained for each time point was standardized with the maximum fluorescence intensity of the ROI during the observation period.

Coinjection of one- and two-arm-PEG-OligoLys

In the coinjection of one- and two-arm-PEG-OligoLys, a mixture of 1.25 mg per mouse of Alexa647-labeled one-arm-PEG-OligoLys and 1.25 mg per mouse of Alexa594-labeled two-arm-PEG-OligoLys was injected from the tail vein. The parenchymal autofluorescence and fluorescence signal from Alexa594 and Alexa647 was detected as described in the "Intravital observation of earlobe and liver" section. After subtracting the background fluorescence intensity, which was measured using the images obtained 10 s before the sample injection, the fluorescence intensity of Alexa594 and Alexa647 was standardized on the basis of the intensity of fluorescence in the blood vessel lumen at 30 s after injection, set to 100% in Fig. 4 (B to D). The attachment of one- and two-arm-PEG-OligoLys to the sinusoidal wall was almost unobservable at 30 s after injection (Fig. 4, A and B).

Blood examination

OligoLys with or without PEGylation was injected into the tail vein at the same dose as for intravital imaging above (1.25 mg per mouse for one- and two-arm-PEG-OligoLys and 0.05 mg per mouse for non-PEGylated OligoLys). Blood was collected from the mice 4 hours after injection to examine the plasma using a DRI-CHEM 7000i system (Fujifilm, Tokyo, Japan).

Ex vivo hemolysis assay

Mouse blood was centrifuged at 500*g* for 5 min to sediment the blood cells, followed by washing with phosphate-buffered saline (PBS; pH 7.4) twice. Red blood cells (RBCs) collected from 1 ml of the blood were suspended in 20 ml of PBS. One volume of OligoLys with or without PEGylation was added to 10 volumes of the RBC suspension. The final concentration of OligoLys with or without PEGylation was adjusted to 7.5 pM, which is the same as the calculated concentration of OligoLys in the blood when OligoLys injected at the dose used in intravital imaging above was evenly distributed in 2 ml of mouse blood. The mixture was incubated at 37°C for 1 hour, followed by centrifugation at 500*g* for 5 min. The absorbance of the supernatant at 405 nm was measured using Microplate Reader Infinite M1000 Pro (Tecan Japan Co. Ltd., Kanagawa, Japan) to quantify the amount of hemoglobin. A mixture of one volume of Triton X-100 (20% v/v) and 10 volumes of RBC suspension was sonicated for use as a positive control (exhibits 100% activity of hemolysis). The absorbance value of each sample was compared to the value obtained for the positive control.

Synthesis of thiol-introduced PEG-PLys

PEG-PLys, used for constructing PM as described in the following section, was synthesized via ROP of L-Lys(TFA)-NCA using PEG-NH_2 (M_n = 12 kDa) (NOF Corporation) as a macroinitiator. The M_w/M_n of PEG-PLys(TFA) was 1.05 according to SEC. The DP of PLys in PEG-PLys was 44, based on the ^{1}H NMR spectrum. The 1-imino-4-mercaptobutyl (IM) groups were introduced onto the side-chain ε-amino groups of the lysine units of the PLys segment in PEG-PLys [PEG-PLys(IM)] using 2-iminothiolane (Thermo Fischer Scientific), according to a previous report (*39*). The introduction ratio of IM in the total NH_2 groups in the original PEG-PLys was 50%, according to the ^{1}H NMR.

Preparation and characterization of PM

A pDNA expressing Luc, pCAG-Luc2, was constructed by cloning the Luc coding sequence of pGL4.13 vector (Promega, Madison, WI, USA) into the pCAG-GS vector (RIKEN BioResource Research Center, Tsukuba, Japan). PM was prepared from PEG-PLys(IM) and pCAG-Luc2 pDNA at [amino groups in PEG-PLys(IM) (N)] to [phosphate groups in pDNA (P)] (N/P) ratio of 2, as previously reported (*39*).

The dynamic light scattering (DLS) and ζ-potential measurements were measured using a Zetasizer Nano ZS ZEN3500 (Malvern Instruments Ltd., Worcestershire, UK). For these measurements, the pDNA concentration was adjusted to 33.3 μg/ml, dissolved in 10 mM Hepes buffer containing 150 mM NaCl for DLS measurement and in 10 mM Hepes buffer without NaCl addition for ζ-potential measurements. The hydrodynamic diameter (D_H) and PDI of PM were evaluated using DLS at a detection angle of 173° and a temperature of 25°C using cumulant methods. The ζ-potential was measured with electrophoretic light scattering at 37°C using Smoluchowski's equation.

For injection, the pDNA concentration was adjusted to 100 μg/ml with a final concentration of Hepes and NaCl of 10 and 150 mM, respectively.

PM observation using IVCLSM

For the intravital imaging of PM, pCAG-Luc2 pDNA was labeled with Cy5 using the Label IT Tracker Intracellular Nucleic Acid Localization Kit (Mirus Bio Corp., Madison, WI). PM loading Cy5-labeled pCAG-Luc2 pDNA was intravenously injected into the tail vein at the dose of 20 μg per mouse 5 min after the intravenous preinjection of two-arm-PEG-OligoLys at a dose of 1.25 mg per mouse. The control mice were injected with 10 mM Hepes buffer containing 150 mM NaCl (pH 7.3) instead of two-arm-PEG-OligoLys solution before PM injection. Liver imaging and the evaluation of the blood circulation profile were performed, as described in the "Intravital observation of earlobe and liver" and "Evaluation of blood circulation profile" sections, respectively.

PM injection into tumor-bearing mice

Murine colon adenocarcinoma 26 (C26) cells were obtained from the National Cancer Center (Tokyo, Japan) and cultured in high-glucose Dulbecco's modified Eagle's medium containing 10% fetal bovine serum. C26 cells (5×10^6 cells per mouse) were inoculated into subcutaneous tissue in the right rear flank of BALB/c nu/nu mice (7 weeks old, female, Charles River Laboratories). Mice with tumors of approximately 100 mm^3 were intravenously injected with PM loading 20 μg of pCAG-Luc2 pDNA, with or without two-arm-PEG-OligoLys preinjection, as described in the previous section. Tumors were harvested 48 hours after PM injection. The extracted tumor was homogenized using Multibeads Shocker in passive lysis buffer (Promega, Madison, WI, USA), followed by a Luc assay using a Luciferase Assay System (Promega) and Lumat LB9507 (Berthold Technologies, Bad Wildbad, Germany). The luminescence intensity values were normalized to the total protein amount in the homogenates determined by the Micro BCA Protein Assay Reagent Kit (Thermo Fischer Scientific). The values were presented after subtracting the background values obtained from the tumors harvested from mice without PM injection.

Luc expression after AAV8 injection

BALB/c mice (6 weeks old, female, Charles River Laboratories) were intravenously injected with 1.25 mg of two-arm-PEG-OligoLys, followed by the injection of AAV8 encoding firefly Luc driven by the CMV-IVS promoter (Vector Biolabs, Malvern, PA, USA) at the dose of 2.5×10^{11} viral genomes per mouse, sequentially at 5-min intervals. For the control mice, 10 mM Hepes buffer containing 150 mM NaCl (pH7.3), instead of two-arm-PEG-OligoLys, was injected before the AAV injection. Three weeks after AAV8 injection, the liver, heart, and muscles from the backside were excised. The Luc assay and data were analyzed as described in the previous section for the quantification of Luc expression in the tumor tissue.

SUPPLEMENTARY MATERIALS

Supplementary material for this article is available at http://advances.sciencemag.org/cgi/content/full/6/26/eabb8133/DC1

View/request a protocol for this paper from *Bio-protocol*.

REFERENCES AND NOTES

1. M. E. Davis, Z. G. Chen, D. M. Shin, Nanoparticle therapeutics: An emerging treatment modality for cancer. *Nat. Rev. Drug Discov.* **7**, 771–782 (2008).
2. T. Lammers, S. Aime, W. E. Hennink, G. Storm, F. Kiessling, Theranostic nanomedicine. *Acc. Chem. Res.* **44**, 1029–1038 (2011).
3. S. Mura, J. Nicolas, P. Couvreur, Stimuli-responsive nanocarriers for drug delivery. *Nat. Mater.* **12**, 991–1003 (2013).
4. V. J. Yao, S. D'Angelo, K. S. Butler, C. Theron, T. L. Smith, S. Marchiò, J. G. Gelovani, R. L. Sidman, A. S. Dobroff, C. J. Brinker, A. R. M. Bradbury, W. Arap, R. Pasqualini, Ligand-targeted theranostic nanomedicines against cancer. *J. Control. Release* **240**, 267–286 (2016).

5. B. Pelaz, C. Alexiou, R. A. Alvarez-Puebla, F. Alves, A. M. Andrews, S. Ashraf, L. P. Balogh, L. Ballerini, A. Bestetti, C. Brendel, S. Bosi, M. Carril, W. C. W. Chan, C. Chen, X. Chen, X. Chen, Z. Cheng, D. Cui, J. Du, C. Dullin, A. Escudero, N. Feliu, M. Gao, M. George, Y. Gogotsi, A. Grünweller, Z. Gu, N. J. Halas, N. Hampp, R. K. Hartmann, M. C. Hersam, P. Hunziker, J. Jian, X. Jiang, P. Jungebluth, P. Kadhiresan, K. Kataoka, A. Khademhosseini, J. Kopeček, N. A. Kotov, H. F. Krug, D. S. Lee, C.-M. Lehr, K. W. Leong, X.-J. Liang, M. L. Lim, L. M. Liz-Marzán, X. Ma, P. Macchiarini, H. Meng, H. Möhwald, P. Mulvaney, A. E. Nel, S. Nie, P. Nordlander, T. Okano, J. Oliveira, T. H. Park, R. M. Penner, M. Prato, V. Puntes, V. M. Rotello, A. Samarakoon, R. E. Schaak, Y. Shen, S. Sjöqvist, A. G. Skirtach, M. G. Soliman, M. M. Stevens, H.-W. Sung, B. Z. Tang, R. Tietze, B. N. Udugama, J. S. VanEpps, T. Weil, P. S. Weiss, I. Willner, Y. Wu, L. Yang, Z. Yue, Q. Zhang, Q. Zhang, X.-E. Zhang, Y. Zhao, X. Zhou, W. J. Parak, Diverse applications of nanomedicine. *ACS Nano* **11**, 2313–2381 (2017).
6. H. Cabral, K. Miyata, K. Osada, K. Kataoka, Block copolymer micelles in nanomedicine applications. *Chem. Rev.* **118**, 6844–6892 (2018).
7. D. E. Owens III, N. A. Peppas, Opsonization, biodistribution, and pharmacokinetics of polymeric nanoparticles. *Int. J. Pharm.* **307**, 93–102 (2006).
8. B. Wang, X. He, Z. Zhang, Y. Zhao, W. Feng, Metabolism of nanomaterials in vivo: Blood circulation and organ clearance. *Acc. Chem. Res.* **46**, 761–769 (2013).
9. K. M. Tsoi, S. A. MacParland, X.-Z. Ma, V. N. Spetzler, J. Echeverri, B. Ouyang, S. M. Fadel, E. A. Sykes, N. Goldaracena, J. M. Kaths, J. B. Conneely, B. A. Alman, M. Selzner, M. A. Ostrowski, O. A. Adeyi, A. Zilman, I. D. McGilvray, W. C. W. Chan, Mechanism of hard-nanomaterial clearance by the liver. *Nat. Mater.* **15**, 1212–1221 (2016).
10. G. Wang, D. Simberg, Role of scavenger receptors in immune recognition and targeting of nanoparticles. *Rev. Cell Biol. Mol. Med.* **1**, 166–189 (2006).
11. K. K. Sørensen, J. Simon-Santamaria, R. S. McCuskey, B. Smedsrød, Liver sinusoidal endothelial cells. *Compr. Physiol.* **5**, 1751–1774 (2015).
12. F. Campbell, F. L. Bos, S. Sieber, G. Arias-Alpizar, B. E. Koch, J. Huwyler, A. Kros, J. Bussmann, Directing nanoparticle biodistribution through evasion and exploitation of stab2-dependent nanoparticle uptake. *ACS Nano* **12**, 2138–2150 (2018).
13. F. Jacobs, E. Wisse, B. De Geest, The role of liver sinusoidal cells in hepatocyte-directed gene transfer. *Am. J. Pathol.* **176**, 14–21 (2010).
14. L. P. Ganesan, S. Mohanty, J. Kim, K. R. Clark, J. M. Robinson, C. L. Anderson, Rapid and efficient clearance of blood-borne virus by liver sinusoidal endothelium. *PLOS Pathog.* **7**, e1002281 (2011).
15. K. Kataoka, A. Harada, Y. Nagasaki, Block copolymer micelles for drug delivery: Design, characterization and biological significance. *Adv. Drug Deliv. Rev.* **47**, 113–131 (2001).
16. A. Soundararajan, A. Bao, W. T. Phillips, R. Perez III, B. A. Goins, [^{186}Re]Liposomal doxorubicin (Doxil): In vitro stability, pharmacokinetics, imaging and biodistribution in a head and neck squamous cell carcinoma xenograft model. *Nucl. Med. Biol.* **36**, 515–524 (2009).
17. J. A. MacKay, M. Chen, J. R. McDaniel, W. Liu, A. J. Simnick, A. Chilkoti, Self-assembling chimeric polypeptide-doxorubicin conjugate nanoparticles that abolish tumours after a single injection. *Nat. Mater.* **8**, 993–999 (2009).
18. Y. Anraku, A. Kishimura, A. Kobayashi, M. Oba, K. Kataoka, Size-controlled long-circulating PICsome as a ruler to measure critical cut-off disposition size into normal and tumor tissues. *Chem. Commun.* **47**, 6054–6056 (2011).
19. M. Ogris, S. Brunner, S. Schüller, R. Kircheis, E. Wagner, PEGylated DNA/transferrin-PEI complexes: Reduced interaction with blood components, extended circulation in blood and potential for systemic gene delivery. *Gene Ther.* **6**, 595–605 (1999).
20. T. Merdan, K. Kunath, H. Petersen, U. Bakowsky, K. H. Voigt, J. Kopecek, T. Kissel, PEGylation of poly(ethylene imine) affects stability of complexes with plasmid DNA under in vivo conditions in a dose-dependent manner after intravenous injection into mice. *Bioconjug. Chem.* **16**, 785–792 (2005).
21. J.-M. Prill, V. Subr, N. Pasquarelli, T. Engler, A. Hoffmeister, S. Kochanek, K. Ulbrich, F. Kreppel, Traceless bioresponsive shielding of adenovirus hexon with HPMA copolymers maintains transduction capacity in vitro and in vivo. *PLOS One* **9**, e82716 (2014).
22. L. Krutzke, J. M. Prill, T. Engler, C. Q. Schmidt, Z. Xu, A. P. Byrnes, T. Simmet, F. Kreppel, Substitution of blood coagulation factor X-binding to Ad5 by position-specific PEGylation: Preventing vector clearance and preserving infectivity. *J. Control. Release* **235**, 379–392 (2016).
23. M. R. A. Abdollah, T. J. Carter, C. Jones, T. L. Kalber, V. Rajkumar, B. Tolner, C. Gruettner, M. Zaw-Thin, J. Baguña Torres, M. Ellis, M. Robson, R. B. Pedley, P. Mulholland, R. T. M. de Rosales, K. A. Chester, Fucoidan prolongs the circulation time of dextran-coated iron oxide nanoparticles. *ACS Nano* **12**, 1156–1169 (2018).
24. H. J. Haisma, J. A. A. M. Kamps, G. K. Kamps, J. A. Plantinga, M. G. Rots, A. R. Bellu, Polyinosinic acid enhances delivery of adenovirus vectors in vivo by preventing sequestration in liver macrophages. *J. Gen. Virol.* **89**, 1097–1105 (2008).
25. M. R. A. Abdollah, T. Kalber, B. Tolner, P. Southern, J. C. Bear, M. Robson, R. B. Pedley, I. P. Parkin, Q. A. Pankhurst, P. Mulholland, K. Chester, Prolonging the circulatory retention of SPIONs using dextran sulfate: In vivo tracking achieved by functionalisation with near-infrared dyes. *Faraday Discuss.* **175**, 41–58 (2014).
26. R. J. Allen, B. Mathew, K. G. Rice, PEG-peptide inhibition of scavenger receptor uptake of nanoparticles by the liver. *Mol. Pharm.* **15**, 3881–3891 (2018).
27. X. Sun, X. Yan, O. Jacobson, W. Sun, Z. Wang, X. Tong, Y. Xia, D. Ling, X. Chen, Improved tumor uptake by optimizing liposome based RES blockade strategy. *Theranostics* **7**, 319–328 (2017).
28. Z. Xu, J. Tian, J. S. Smith, A. P. Byrnes, Clearance of adenovirus by Kupffer cells is mediated by scavenger receptors, natural antibodies, and complement. *J. Virol.* **82**, 11705–11713 (2008).
29. S. Alidori, R. L. Bowman, D. Yarilin, Y. Romin, A. Barlas, J. J. Mulvey, S. Fujisawa, K. Xu, A. Ruggiero, V. Riabov, D. L. J. Thorek, H. D. S. Ulmert, E. J. Brea, K. Behling, J. Kzhyshkowska, K. Manova-Todorova, D. A. Scheinberg, M. R. McDevitt, Deconvoluting hepatic processing of carbon nanotubes. *Nat. Commun.* **7**, 12343 (2016).
30. H. Y. Hsu, S. L. Chiu, M. H. Wen, K. Y. Chen, K. F. Hua, Ligands of macrophage scavenger receptor induce cytokine expression via differential modulation of protein kinase signaling pathways. *J. Biol. Chem.* **276**, 28719–28730 (2001).
31. S. Marshall-Clarke, J. E. Downes, I. R. Haga, A. G. Bowie, P. Borrow, J. L. Pennock, R. K. Grencis, P. Rothwell, Polyinosinic acid is a ligand for toll-like receptor 3. *J. Biol. Chem.* **282**, 24759–24766 (2007).
32. K. Walton, Experiments with dextran sulphate as an anticoagulant. *Proc. R. Soc. Med.* **44**, 563–564 (1951).
33. J. L. Stow, L. Kjéllen, E. Unger, M. Höök, M. G. Farquhar, Heparan sulfate proteoglycans are concentrated on the sinusoidal plasmalemmal domain and in intracellular organelles of hepatocytes. *J. Cell Biol.* **100**, 975–980 (1985).
34. R. S. Burke, S. H. Pun, Extracellular barriers to in vivo PEI and PEGylated PEI polyplex-mediated gene delivery to the liver. *Bioconjug. Chem.* **19**, 693–704 (2008).
35. Z. Kadlecova, L. Baldi, D. Hacker, F. M. Wurm, H.-A. Klok, Comparative study on the in vitro cytotoxicity of linear, dendritic, and hyperbranched polylysine analogues. *Biomacromolecules* **13**, 3127–3137 (2012).
36. M. A. Gosselin, W. Guo, R. J. Lee, Efficient gene transfer using reversibly cross-linked low molecular weight polyethylenimine. *Bioconjug. Chem.* **12**, 989–994 (2001).
37. T. Yamaoka, Y. Tabata, Y. Ikada, Distribution and tissue uptake of poly(ethylene glycol) with different molecular weights after intravenous administration to mice. *J. Pharm. Sci.* **83**, 601–606 (1994).
38. J. W. Smit, A. H. Schinkel, B. Weert, D. K. F. Meijer, Hepatobiliary and intestinal clearance of amphiphilic cationic drugs in mice in which both *mdr1a* and *mdr1b* genes have been disrupted. *Br. J. Pharmacol.* **124**, 416–424 (1998).
39. K. Miyata, Y. Kakizawa, N. Nishiyama, A. Harada, Y. Yamasaki, H. Koyama, K. Kataoka, Block catiomer polyplexes with regulated densities of charge and disulfide cross-linking directed to enhance gene expression. *J. Am. Chem. Soc.* **126**, 2355–2361 (2004).
40. K. M. Takeda, Y. Yamasaki, A. Dirisala, S. Ikeda, T. A. Tockary, K. Toh, K. Osada, K. Kataoka, Effect of shear stress on structure and function of polyplex micelles from poly(ethylene glycol)-poly(L-lysine) block copolymers as systemic gene delivery carrier. *Biomaterials* **126**, 31–38 (2017).
41. M. Oba, Y. Vachutinsky, K. Miyata, M. R. Kano, S. Ikeda, N. Nishiyama, K. Itaka, K. Miyazono, H. Koyama, K. Kataoka, Antiangiogenic gene therapy of solid tumor by systemic injection of polyplex micelles loading plasmid DNA encoding soluble Flt-1. *Mol. Pharm.* **7**, 501–509 (2010).
42. Y. Vachutinsky, M. Oba, K. Miyata, S. Hiki, M. R. Kano, N. Nishiyama, H. Koyama, K. Miyazono, K. Kataoka, Antiangiogenic gene therapy of experimental pancreatic tumor by sFlt-1 plasmid DNA carried by RGD-modified crosslinked polyplex micelles. *J. Control. Release* **149**, 51–57 (2011).
43. C. Hinderer, N. Katz, E. L. Buza, C. Dyer, T. Goode, P. Bell, L. K. Richman, J. M. Wilson, Severe toxicity in nonhuman primates and piglets following high-dose intravenous administration of an adeno-associated virus vector expressing human SMN. *Hum. Gene Ther.* **29**, 285–298 (2018).
44. Z. Wang, T. Zhu, C. Qiao, L. Zhou, B. Wang, J. Zhang, C. Chen, J. Li, X. Xiao, Adeno-associated virus serotype 8 efficiently delivers genes to muscle and heart. *Nat. Biotechnol.* **23**, 321–328 (2005).
45. H. T. McMahon, E. Boucrot, Molecular mechanism and physiological functions of clathrin-mediated endocytosis. *Nat. Rev. Mol. Cell Biol.* **12**, 517–533 (2011).
46. J. Rejman, V. Oberle, I. S. Zuhorn, D. Hoekstra, Size-dependent internalization of particles via the pathways of clathrin- and caveolae-mediated endocytosis. *Biochem. J.* **377**, 159–169 (2004).
47. S. Alexander, Adsorption of chain molecules with a polar head a scaling description. *J. Phys. France* **38**, 983–987 (1977).
48. P. G. de Gennes, Conformations of polymers attached to an interface. *Macromolecules* **13**, 1069–1075 (1980).
49. S. Watanabe, K. Hayashi, K. Toh, H. J. Kim, X. Liu, H. Chaya, S. Fukushima, K. Katsushima, Y. Kondo, S. Uchida, S. Ogura, T. Nomoto, H. Takemoto, H. Cabral, H. Kinoh, H. Y. Tanaka, M. R. Kano, Y. Matsumoto, H. Fukuhara, S. Uchida, M. Nangaku, K. Osada, N. Nishiyama,

K. Miyata, K. Kataoka, In vivo rendezvous of small nucleic acid drugs with charge-matched block catiomers to target cancers. *Nat. Commun.* **10**, 1894 (2019).
50. A. Dirisala, S. Uchida, T. A. Tockary, N. Yoshinaga, J. Li, S. Osawa, L. Gorantla, S. Fukushima, K. Osada, K. Kataoka, Precise tuning of disulphide crosslinking in mRNA polyplex micelles for optimising extracellular and intracellular nuclease tolerability. *J. Drug Target.* **27**, 670–680 (2019).
51. O. F. Mutaf, A. Kishimura, Y. Mochida, A. Kim, K. Kataoka, Induction of secondary structure through micellization of an oppositely charged pair of homochiral block- and homopolypeptides in an aqueous medium. *Macromol. Rapid Commun.* **36**, 1958–1964 (2015).
52. G. L. Kenausis, J. Vörös, D. L. Elbert, N. Huang, R. Hofer, L. Ruiz-Taylor, M. Textor, J. A. Hubbell, N. D. Spencer, Poly($_L$-lysine)-*g*-poly(ethylene glycol) layers on metal oxide surfaces: Attachment mechanism and effects of polymer architecture on resistance to protein adsorption. *J. Phys. Chem. B* **104**, 3298–3309 (2000).

Acknowledgments: We thank M. Kuronuma and Y. Satoh (Kawasaki Institute of Industrial Promotion) for technical assistance. **Funding:** This research was supported financially by the Japan Science and Technology Agency (JST) through the Center of Innovation (COI) Program [Center of Open Innovation Network for Smart Health (COINS) (grant number JPMJCE1305)], Research on the Innovative Development and the Practical Application of New Drugs for Hepatitis B from the Japan Agency for Medical Research and Development (AMED) (JP17fk0310111 to K.K.), and Grants-in-Aid for Scientific Research (B) (18 K03529 to S.U.) and for Early-Career Scientist (18 K18393 to A.D.) from the Ministry of Education, Culture, Sports, Science and Technology, Japan (MEXT). **Author contributions:** A.D., S.U., and K.K conceived the idea, designed all the experiments, and wrote the manuscript. A.D. performed all the experiments. K.T. helped with the IVCLSM experiments. S.A. performed the pharmacokinetic analysis. H.K. assisted with the virus experiment. S.F. helped with synthesis of the oligocations. J.L., S.O., T.A.T., X.L., K.H., and Y.M. contributed in the other experiments. K.O. discussed the experimental data. S.U. and K.K. supervised the whole project. **Competing interests:** K.K. is a founder and a scientific advisor of AccuRna Inc. The remaining authors declare that they have no conflict of interests. PCT patent pending: Kawasaki Institute of Industrial Promotion (K.K., S.O., S.U., K.H., A.D., and K.T). Date: 12 March 2019; serial numbers: PCT/JP2019/009919. JP patent pending: Kawasaki Institute of Industrial Promotion (K.K., S.O., S.U., K.H., and K.O). Date: 19 November 2019; serial numbers: JP2019/520319**. Data and materials availability:** All experimental data needed to evaluate the conclusions in the paper are present in the paper and/or the Supplementary Materials. Additional data related to this paper may be requested are from the authors.

Submitted 20 March 2020
Accepted 13 May 2020
Published 26 June 2020
10.1126/sciadv.abb8133

Citation: A. Dirisala, S. Uchida, K. Toh, J. Li, S. Osawa, T. A. Tockary, X. Liu, S. Abbasi, K. Hayashi, Y. Mochida, S. Fukushima, H. Kinoh, K. Osada, K. Kataoka, Transient stealth coating of liver sinusoidal wall by anchoring two-armed PEG for retargeting nanomedicines. *Sci. Adv.* **6**, eabb8133 (2020).